Histol Histopathol (2022) 37: 971-983

http://www.hh.um.es

Histology and Histopathology
From Cell Biology to Tissue Engineering

ORIGINAL ARTICLE **Open Access**

Circular RNA circSDHC (hsa_circ_0015004) regulates tumor growth and angiogenesis via regulating centrosomal protein 55 expression in renal cell carcinoma

Long Pei, Chunhui Dong, Yanchao Wang, Xianqiang Lv, Gaopei Jia and Aili Zhang

Department of Urology, The Fourth Hospital of Hebei Medical University, Shijiazhuang City, Hebei Province, China

Summary. Background. Renal cell carcinoma (RCC) is the main aggressive subtype of kidney cancer. Circular RNAs have been shown to exert critical roles in RCC. However, little is known about the regulatory mechanism of hsa_circ_0015004 (circSDHC) in RCC.

Methods. 35 patients with RCC were recruited in the research. Expression changes of circSDHC were determined by real-time quantitative polymerase chain reaction (RT-qPCR). The effects of circSDHC inhibition on cell proliferation, apoptosis, angiogenesis, migration, and invasion were analyzed. The regulation mechanism of circSDHC was surveyed by bioinformatics analysis. The effect of circSDHC on tumorigenesis was validated by xenograft assay.

Results. We observed an observable elevation in circSDHC expression in RCC tissues and cell lines. Functionally, circSDHC silencing decreased xenograft tumor growth and induced RCC cell apoptosis, repressed RCC cell proliferation, angiogenesis, migration, and invasion *in vitro*. Mechanically, circSDHC modulated centrosomal protein 55 (CEP55) expression by functioning as a miR-130a-3p sponge. Also, miR-130a-3p silencing offset circSDHC knockdown-mediated impacts on malignant phenotypes and angiogenesis of RCC cells. Furthermore, exogenetic expression of CEP55 counteracted miR-130a-3p overexpression-mediated effects on malignant phenotypes and angiogenesis of RCC cells.

Conclusion. Silencing of circSDHC restrained cell malignant phenotypes and angiogenesis via reducing CEP55 expression by releasing miR-130a-3p in RCC, providing a new mechanism for understanding the progression of RCC.

Corresponding Author: Aili Zhang, Department of Urology, The Fourth Hospital of Hebei Medical University, 050000, No. 12, Jiankang Road, Chang'an District, Shijiazhuang City, 050000, Hebei Province, China. e-mail: mnwkpl6688@163.com

DOI: 10.14670/HH-18-467

Key words: RCC, circSDHC, miR-130a-3p, CEP55

Introduction

Renal cell carcinoma (RCC), the third most common urogenital malignancy, accounts for approximately 2% to 3% of all adult malignancies (Petejova and Martinek, 2016; Gudowska-Sawczuk et al., 2020). There is a good prognosis in patients with RCC at the early-stage, but as many as 10% of patients relapse after surgery (Izumi et al., 2020). Once metastasis occurs, the prognosis of RCC patients is extremely poor (Pal et al., 2017; Lee et al., 2021; Roberto et al., 2021). Therefore, exploring the mechanisms of RCC progression is crucial for developing therapeutic strategies.

Circular RNAs (circRNAs), generated through alternative splicing events, are single-stranded RNA transcripts with covalently circular-closed structures (Ebbesen et al., 2017). CircRNAs have extraordinary stability due to the lack of free ends that are prone to exonuclease degradation (Suzuki et al., 2006). Also, numerous circRNAs are regulated in pathophysiological conditions and developmental stages (Santer et al., 2019). A large amount of evidence indicates that circRNAs are implicated in certain renal diseases, such as diabetic nephropathy, acute kidney injury, and RCC (Jin et al., 2020). For instance, circRNA-PTCH1 and circRNA-TLK1 play a promoting effect on RCC cell invasion and migration (Liu et al., 2020; Li et al., 2020a). CircRNA-SDHC (circSDHC), also termed as hsa_circ_0015004, is overexpressed in RCC in two datasets GSE100186 and GSE137836. Also, circSDHC has been proved to facilitate RCC cell invasion and proliferation (Cen et al., 2021). Nevertheless, the role and regulatory mechanism of circSDHC in RCC have not been fully investigated. Emerging evidence suggests that circRNAs are functional molecules and exert their functions by acting as microRNAs (miRNAs) or protein

©The Author(s) 2022. **Open Access.** This article is licensed under a Creative Commons CC-BY International License.

inhibitors ("sponges") (Kristensen et al., 2019). MiRNAs, another cluster of single-stranded RNA molecules, are key regulators in diverse biological processes related to RCC progression (Kovacova et al., 2018; Nogueira et al., 2018; Ghafouri-Fard et al., 2020). MiR-130a-3p exerts a tumor-inhibiting function in certain cancers, such as liver cancer (Wang et al., 2017), bladder cancer (Zhu et al., 2021), and breast cancer (Zhong et al., 2020). Analogously, miR-130a-3p plays an inhibitory impact on tumor growth in RCC (Jing et al., 2021). Nevertheless, the relationship between circSDHC and miR-130a-3p in RCC is unclear.

CEP55, also known as c10orf3 and FLJ10540, is a coiled-coil centrosomal protein (Tandon and Banerjee, 2020). It is required for transport and ALIX binding domain functions and plays a critical role in cytokinetic abscission during mitotic exit (Lee et al., 2008). CEP55 upregulation has been uncovered to be correlated with metastasis, aggressiveness, tumor stage, and poor prognosis across multiple tumor types (Jeffery et al., 2016). It has been reported that CEP55 serves as a potential prognostic and diagnostic biomarker for clear cell RCC (Zhou et al., 2019). Also, CEP55 upregulation activates the PI3K/AKT/mTOR pathway that regulates cell growth migration, survival, angiogenesis and metabolism, and tumorigenesis (Miricescu et al., 2021), resulting in facilitating RCC cell epithelial-mesenchymal transition (Chen et al., 2019). At present, the network mechanisms that regulate CEP55 are still unclear in RCC.

Accordingly, the study was to probe into whether circSDHC mediates RCC progression through the miR-130a-3p/CEP55 axis by functioning as a miR-130a-3p sponge. Notably, circSDHC facilitated cell malignant phenotypes and angiogenesis via sequestering miR-130a-3p and elevating CEP55 expression. This study provided important evidence for elucidating the management of circSDHC on RCC progression.

Materials and methods

Ethics statement

The use of human clinical samples was approved by the Ethics Committee of The Fourth Hospital of Hebei Medical University. 35 patients were diagnosed with RCC in the The Fourth Hospital of Hebei Medical University and underwent surgery under the condition of signing informed consent. Collection of clinical samples from RCC patients was performed according to the Declaration of Helsinki, including RCC tissues and paired normal tissues. Information on 35 patients had been provided in Table 1.

Cell culture

RCC cell lines A498 (#CL-0254) and 786-O (#CL-0010), an immortalized proximal tubule cell line (HK2) (#CL-0109), and human umbilical vein endothelial cell line HUVEC (#CL-0122) were bought from Procell (Wuhan, China). 786-O and HK2 cell lines were cultured in MEM (#PM150410, Procell), the A498 cell line was maintained in RPMI-1640 medium (#PM150110, Procell), and the HUVEC cell line was cultured in Ham's F-12K(#PM150910, Procell). These mediums were supplemented with 10% fetal bovine serum (#164210-500, Procell) and 1% penicillin and streptomycin solution (#PB180120, Procell). Additionally, Ham's F-12K was supplemented with 0.1 mg/mL heparin (Sigma, St. Louis, MO, USA) and 0.05 mg/mL endothelial cell growth supplement (Sigma). All cells were grown in an incubator with 5% CO_2 at 37°C.

Transfection

RCC cell lines were transfected with siRNA against circSDHC (si-circSDHC) (50 nM), negative control for siRNA (si-NC) (50 nM), miR-130a-3p inhibitor (20 nM), miR-NC inhibitor (20 nM), miR-130a-3p mimic (20 nM), miR-NC mimic (20 nM), circSDHC overexpression plasmid (oe-circSDHC) (2 μg), negative control for oe-circSDHC (vector) (2 μg), CEP55 overexpression plasmid (CEP55) (2 μg), or negative control for CEP55 (pcDNA) (2 μg) using jetPRIME transfection reagent (Polyplus, Illkirch, France). Nucleotide sequences are provided in Table 2. The circSDHC and CEP55 overexpression plasmids were generated using empty pCD5-ciR (Geneseed,

Table 1. Correlations between circSDHC expression levels and clinicopathological characteristics in RCC.

Characteristics	CircSDHC expression		*p*-value
	Low (n=17)	High (n=18)	
Age (years)			0.7332
<60	10	12	
≥60	7	6	
Gender			ns
Male	12	13	
Female	5	5	
AJ CC stage_T			0.0275*
T1/T2	15	9	
T3/T4	2	9	
AJCC stage_N			0.0858
N0	13	8	
N1	4	10	
AJCC stage_M			0.3175
M0	10	7	
M1	7	11	
STAGE			0.0354*
I/II	14	8	
III/IV	3	10	
GRADE			0.5051
I/II	8	11	
III/IV	9	7	

*$p<0.05$ was considered to be statistically significant (chi-square test). AJCC American Joint Committee on Cancer.

Guangzhou, China) and pcDNA (Thermo Fisher, Waltham, MA, USA) vectors, respectively.

RT-qPCR

Extraction of total RNA from clinical samples and cultured cells was performed using the NucleoSpin RNA/protein kit (Macherey-Nagel, Düren, Germany) following the operating procedures provided by the manufacturer. Nuclear RNA and cytoplasmic RNA were isolated from RCC cell lines with the PARIS kit (Thermo Fisher) as the manufacturer's instructions. Complementary DNA was reverse-transcribed from the total RNA using the HiScript II 1st Strand cDNASynthesis Kit (Vazyme, Nanjing, China) or miRNA 1st Strand cDNA Synthesis Kit (Vazyme). QPCR was executed using a ChamQ Universal SYBR® qPCR Master Mix (Vazyme) with specific primers (Table 3). Data were analyzed using the $2^{-\Delta\Delta Ct}$ method and normalized to β-Actin or U6 housekeeping gene.

5-ethynyl-2'-deoxyuridine (EdU) incorporation assay

Cell proliferation was evaluated using the Cell-Light EdU Apollo488 kit (RiboBio, Guangzhou, China) following the operating procedures provided by the manufacturer. In short, RCC cell lines were incubated with 50 μM EdU for 2 h after 24 h of transfection. Subsequently, the cells were fixed by 4% paraformaldehyde (RiboBio) for 30 min and then incubated with 1× Apollo for 30 min in the dark. Cell nuclei were stained using the DAPI solution (Thermo Scientific). The images were acquired using a fluorescence photomicroscope (Carl Zeiss, Oberkochen, Germany). The proportion of EdU-positive cells was calculated in at least five random fields.

Cell apoptosis analysis

Apoptosis was evaluated using Annexin V-FITC and propidium iodide (PI) Apoptosis Detection Kit (Solarbio, Beijing, China) according to the manufacturer's instructions. Cultured cells were digested with EDTA-free trypsin and harvested. 1× Binding Buffer was used to resuspend cells at a concentration of 5×10^6/mL. 100 μL of cell suspension was stained with 5 μL Annexin V-FITC and 5 μL PI at room temperature in the dark. A FACScan flow cytometer (BD Biosciences, San Jose, CA, USA) was utilized for sample analysis.

Western blotting

Extraction of total protein from clinical samples and cultured cells was carried out using the NucleoSpin RNA/protein kit (Macherey-Nagel) based on the manufacturer's procedures. 20 μg total protein was loaded on 10% polyacrylamide gel, followed by transferring to a nitrocellulose membrane (Thermo Fisher). Membranes were recognized with primary antibodies after blocking with 5% non-fat milk. Subsequently, the membranes were incubated with a secondary antibody. Blots were developed by ECL Western Blot Kit (Thermo Fisher). All antibodies were: Bax (#5023, 1:1000, CST, Danvers, MA, USA), Bcl-2 (#4223, 1:1000, CST), CEP55 (#81693, 1:1000, CST), β-Actin (#4967, 1:1000, CST), and goat anti-rabbit IgG (#7074, 1:3000, CST).

HUVEC tube formation assay

HUVECs (Procell) were suspended in conditioned mediums in which RCC cell lines were cultured, followed by seeding on a 24-well plate coated with matrigel (BD Biosciences, 300 μL/well). 6 h later, tube formation was photographed using microscopy (Olympus, Tokyo, Japan). Tube formation was evaluated by ImageJ software (v.8.0, NIH, Bethesda, MD, USA).

Transwell assay

Transwell chambers (Costar, Cambridge, MA, USA) were used to evaluate RCC cell migration and invasion. After transfection for 24 h, the cells (1×10^5) were suspended in 200 μL serum-free medium and placed on the apical chamber without or pre-coated with matrigel (BD Biosciences) in migration and invasion analysis, respectively. 600 μL medium encompassing 10% fetal bovine serum (Procell) was added to the basolateral

Table 2. Sequences used for transfection.

Name	Sequence (5'-3')
si-circSDHC	AACGUGUCAAGUGUCGGAU
si-NC	UUCUCCGAACGUGUCACGUTT
miR-130a-3p inhibitor	AUGCCCUUUUAACAUUGCACUG
miR-NC inhibitor	UCUACUCUUUCUAGGAGGUUGUGA
miR-130a-3p mimic	CAGUGCAAUGUUAAAAGGGCAU
miR-NC mimic	UCACAACCUCCUAGAAAGAGUAGA

Table 3. Primers for RT-qPCR used in the study.

Genes	Primer sequences (5'-3')
circSDHC	Forward (F): 5'-TGTGAAGTCCCTGTGTCTGG-3' Reverse (R): 5'-TTCCCAAAGGAACAGCATTT-3'
β-Actin	F: 5'-CAGCCATGTACGTTGCTATCCA-3' R: 5'-TCACCGGAGTCCATCACGAT-3'
18S rRNA	F: 5'-GTGGTGTTGAGGAAAGCAGACA-3' R: 5'-TGATCACACGTTCCACCTCATC-3'
U6	F: 5'-CTCGCTTCGGCAGCACA-3' R: 5'-AACGCTTCACGAATTTGCGT-3'
CEP55	F: 5'-TCGACCGTCAACATGTGCAGCA-3' R: 5'-GGCTCTGTGATGGCAAACTCATG-3'
miR-130a-3p	F: 5'-CGCGCAGTGCAATGTTAAAA-3' R: 5'-AGTGCAGGGTCCGAGGTATT-3'

chamber. 24 h later, the migratory and invaded cells were allowed to stain with 0.1% crystal violet (Beyotime), followed by counting under a microscope (Olympus).

Dual-luciferase reporter assay

RCC cell lines were co-transfected with miR-130a-3p mimic or miR-NC mimic and a luciferase reporter containing WT-circSDHC, MUT-circSDHC, WT-CEP55 3'UTR, or MUT-CEP55 3'UTR. Luciferase reporters were generated by ligating the fragments of wild-type circSDHC and CEP55 3'UTR and their mutant sequences into the psiCHECK-2 vector (Promega, Madison, WI, USA), respectively. 2 days later, the supernatants of the cell lysates were used for analysis of luciferase activities using a dual luciferase assay system (Promega). Relative luciferase activities were normalized to the *Renilla* luciferase activity.

In vivo experiments

The animal experiments were conducted with the permission approved by the Animal Ethics Committee of The Fourth Hospital of Hebei Medical University. Male nude mice (BALB/c, 4-week-old) (Vital River Laboratory, Beijing, China) were allowed to adapt to the environment for a week (specific pathogen-free environment). 10 mice (5 mice in each group) were subcutaneously injected with A498 cells infected with lentivirus particles carrying sh-circSDHC or sh-NC. Tumor volume was measured once a week. After 4 weeks, the mice were killed, followed by excision of xenograft tumors and weighing. The tumor volumes were determined by measuring the length and width and calculating as volume=(length ×width^2)/2.

Immunohistochemistry (IHC) analysis

IHC analysis of paraffin-embedded xenograft tumor sections was executed using an IHC staining kit (ZSGB-Bio, Beijing, China) according to the manufacturer's procedures. Tissue sections were deparaffinized, dehydrated, washed with PBS and then subjected to antigen retrieval in boiling citrate buffer (pH 6.0). Following 1 h of blocking with 5% normal goat serum, sections were incubated with rabbit anti-CEP55 (#23891-1-AP, Thermo Fisher) at a dilution of 1:50 overnight. Goat anti-rabbit IgG/horseradish peroxidase was used as a secondary antibody (#31466, Thermo

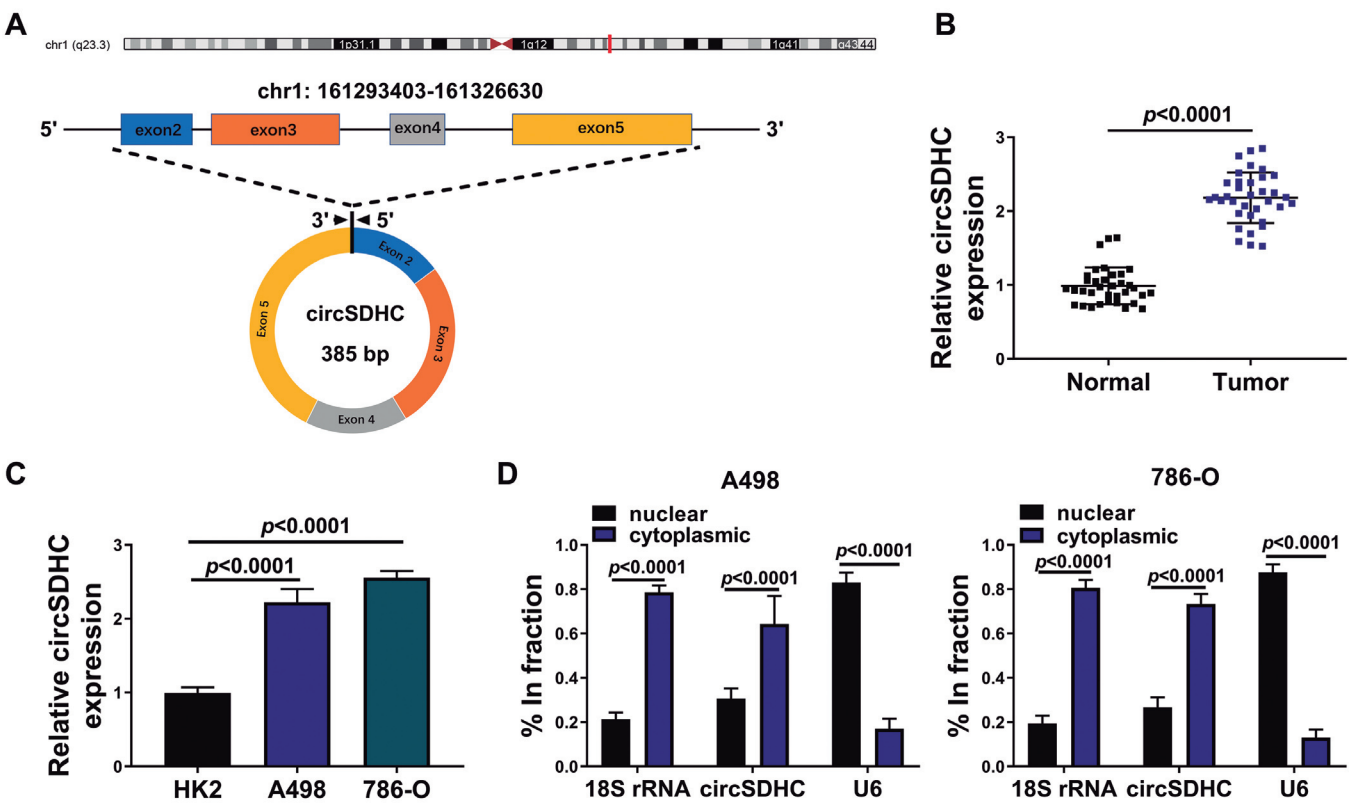

Fig. 1. The expression changes of circSDHC in RCC and its distribution in RCC cell lines. **A.** Schematic illustration of the genomic location of circSDHC. **B, C.** Relative levels of circSDHC in RCC samples and cell lines were evaluated. **D.** Nuclear-cytoplasmic fractionation assays analysis of the localization of circSDHC in RCC cell lines. The U6 and 18S rRNA genes were used as positive controls for the nucleus and cytoplasm, respectively. ****P<0.0001.

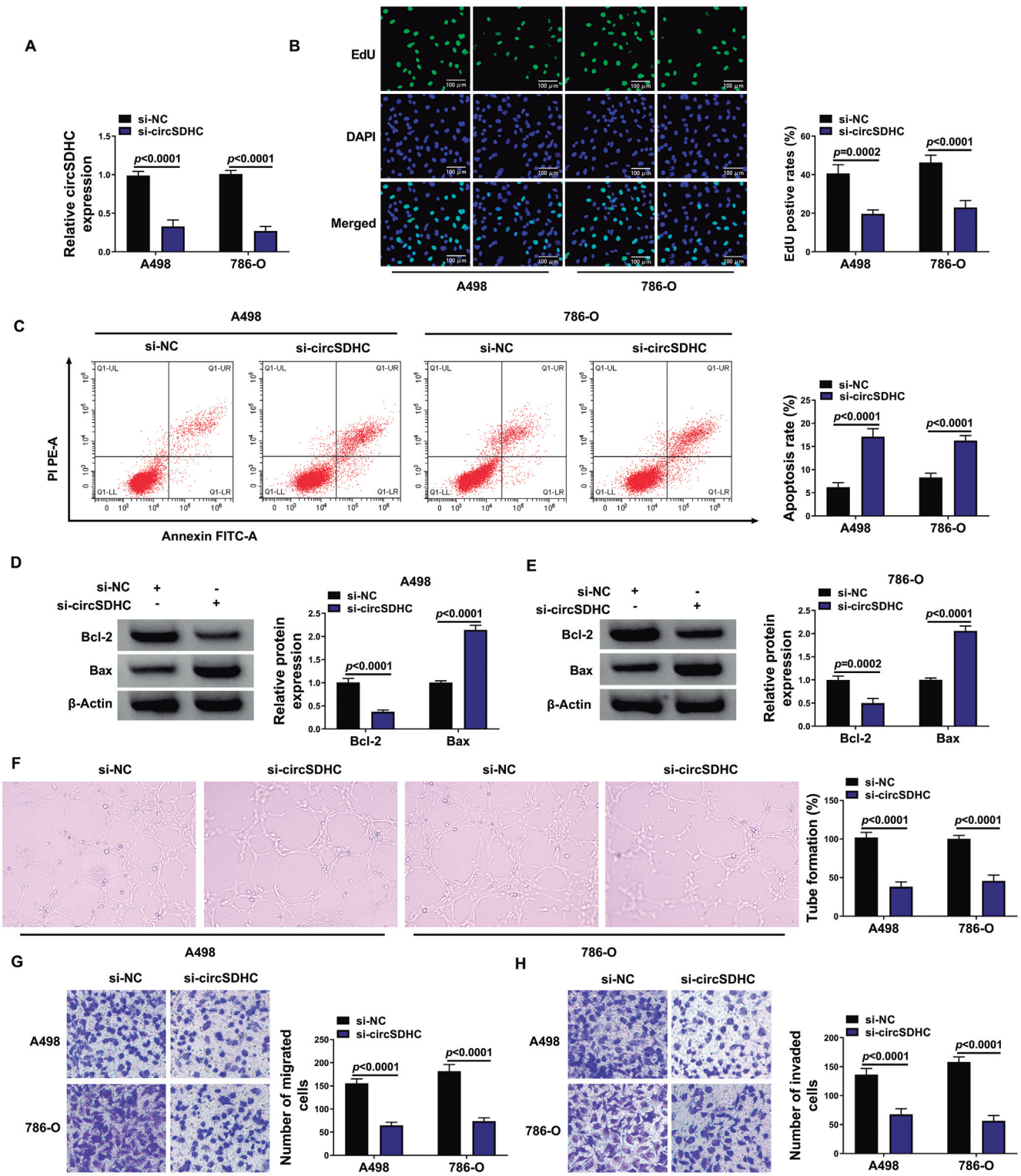

Fig. 2. Interference of circSDHC reduced malignant phenotypes and angiogenesis of RCC cell lines. **A.** The silencing efficiency of si-circSDHC on circSDHC in RCC cell lines was evaluated. **B, C.** Cell proliferation and apoptosis were detected in circSDHC-silenced RCC cell lines and their control cells using EdU and flow cytometry assays. **D, E.** Relative protein levels of Bcl-2 and Bax in circSDHC-silenced RCC cell lines and their control cells were measured using western blotting. **F.** HUVEC tube formation assays were performed to detect tube-like structure formation in HUVECs, which were incubated with conditioned medium for culturing circSDHC-silenced RCC cell lines or their control cells. **G, H.** Cell migration and invasion were analyzed in circSDHC-silenced RCC cell lines or their control cells using transwell assays. ***P*<0.001 and *****P*<0.0001.

Fisher). Finally, immune complexes were visualized using diaminobenzidine, and sections were counterstained with hematoxylin. Images were taken on a fluorescence photomicroscope (Carl Zeiss).

Statistical analysis

All experiments were performed with at least 3 biological replicates. Statistical significance was analyzed using Student's t-tests for two groups or one-way and two-way analysis of variance (ANOVA) for multiple groups in GraphPad Prism 8 (GraphPad Software, San Diego, CA, USA). Multiple comparisons between experimental groups were adjusted using Tukey's multiple comparison test. Asterisks indicated significant differences between experimental groups (***P*<0.01, ****P*<0.001, and ****P*<0.001).

Results

Increased expression of circSDHC in RCC tissues and cells

It has been reported that circSDHC plays a oncogenic function in RCC (Cen et al., 2021). CircSDHC, derived from the SDHC locus, is formed by reverse splicing of exons 2 to 5 (Fig. 1A). To verify the function of circSDHC in RCC, the changes of circSDHC in RCC were detected. Data in Fig. 1B presents that circSDHC was strongly expressed in RCC tissues relative to paired normal tissues (p<0.0001). Also, RCC patients with high circSDHC expression were associated with AJCC stage_N (p=0.0361) and STAGE (P=0.0414) (Table 1). Analogously, circSDHC had higher levels in RCC cell lines (A498 and 786-O) than that in the HK2

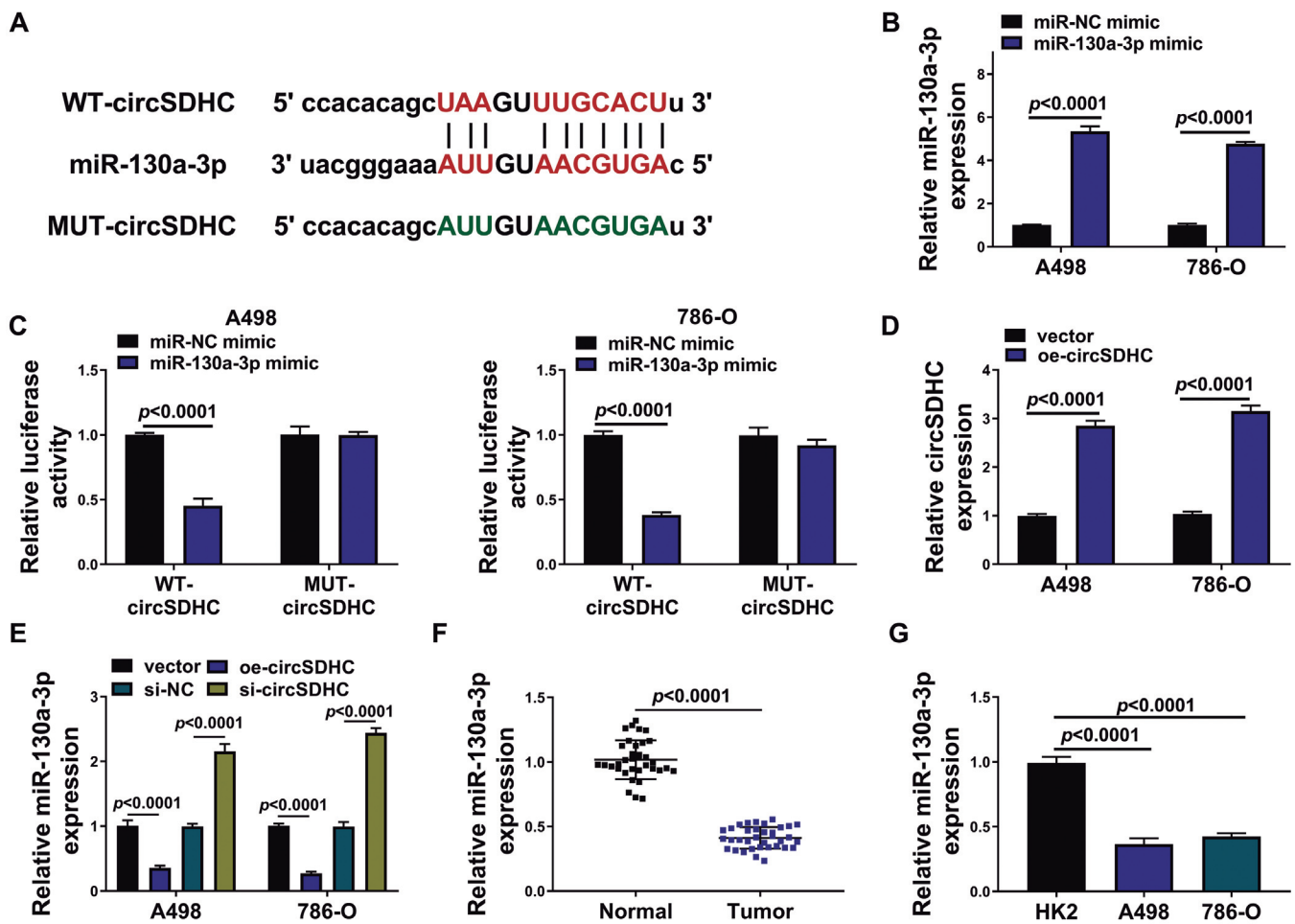

Fig. 3. CircSDHC functioned as a miR-130a-3p decoy. **A.** The putative binding sites between circSDHC and miR-130a-3p. **B.** The transfection efficiency of miR-130a-3p mimic in RCC cell lines was evaluated. **C.** The luciferase activity of wild-type or mutant circSDHC reporter in RCC cell lines with miR-NC mimic or miR-130a-3p mimic. **D.** The transfection efficiency of oe-circSDHC in RCC cell lines was evaluated by RT-qPCR. **E.** Relative expression of miR-130a-3p in RCC cell lines transfected with si-NC, si-circSDHC, oe-circSDHC, or vector was analyzed using RT-qPCR. **F, G.** Relative levels of miR-130a-3p in RCC tissues and cell lines were detected using RT-qPCR. *****P*<0.0001.

cell line (p<0.0001) (Fig. 1C). We then analyzed the distribution of circSDHC in RCC cell lines. Nuclear/cytoplasmic fractionation assay showed that circSDHC was mainly localized in the cytoplasm (p<0.0001) (Fig. 1D). Collectively, circSDHC was upregulated in RCC and it was predominantly distributed in the cytoplasm.

CircSDHC promoted malignant phenotypes and angiogenesis of RCC cell lines

Based on the upregulation of circSDHC in RCC, we knocked down circSDHC in RCC cell lines using a siRNA to validate the function of circSDHC. There was a significant decrease in circSDHC expression in RCC cell lines transfected with si-circSDHC (p<0.0001) (Fig. 2A). EdU and flow cytometry assays showed that circSDHC knockdown markedly impaired RCC cell proliferation (p=0.0002 and p<0.0001) and induced RCC cell apoptosis (p<0.0001) (Fig. 2B,C). Western blotting showed that circSDHC silencing decreased Bcl-2 protein levels (p<0.0001 and p=0.0002) in RCC cell lines, whereas it elevated Bax protein levels (p<0.0001) (Fig. 2D,E). Tube formation assay indicated that circSDHC silencing restrained RCC cell tube formation (p<0.0001) (Fig. 2F). Also, knockdown of circSDHC led to a repression in RCC cell migration and invasion, as demonstrated by transwell assays (p<0.0001) (Fig. 2G,H). Together, inhibition of circSDHC decreased malignant phenotypes and angiogenesis of RCC cell lines.

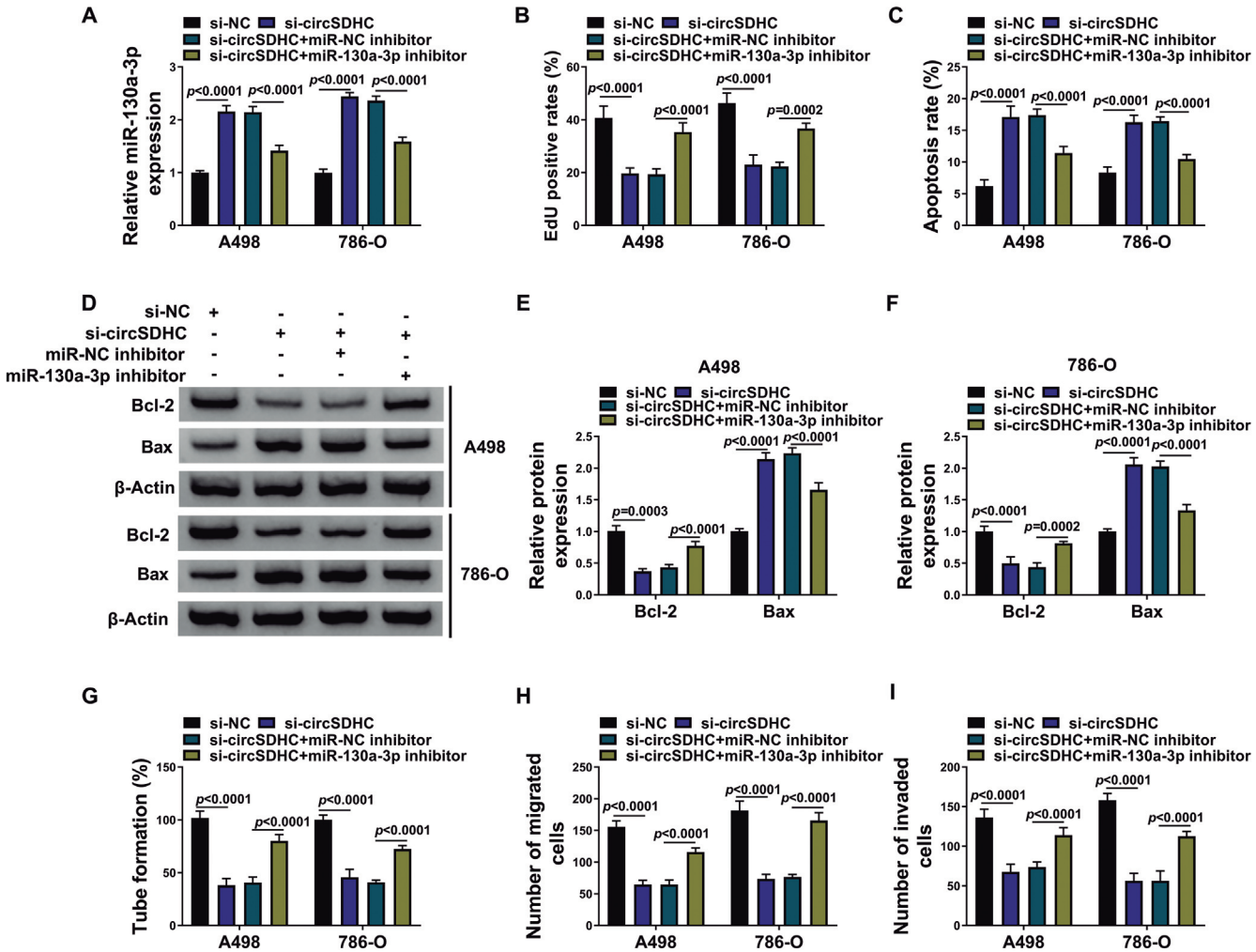

Fig. 4. CircSDHC regulated RCC cell malignant phenotypes and angiogenesis by acting as a miR-130a-3p sponge. **A.** Effect of miR-130a-3p inhibitor on miR-130a-3p expression in circSDHC-inhibited RCC cell lines was analyzed. **B, C.** Impacts of miR-130a-3p knockdown on proliferation and apoptosis of circSDHC-inhibited RCC cell lines were determined using EdU and flow cytometry assays. **D-F.** Effects of miR-130a-3p silencing on Bcl-2 and Bax protein levels in circSDHC-silenced RCC cell lines were evaluated using western blotting. **G-I.** Impacts of miR-130a-3p silencing on tube formation, migration, and invasion were analyzed using HUVEC tube formation and transwell assays. ***P<0.001 and ****P<0.0001.

CircSDHC acted as a miR-130a-3p sponge

Based on the predominant distribution of circSDHC in RCC cell lines, we further analyzed whether circSDHC could function as a sponge for miRNAs. Through bioinformatics prediction (starbase), literature review, and preliminary experiments, miR-130a-3p, which has a complementary sequence to circSDHC, was selected to be further analyzed (Fig. 3A). To validate this prediction, we used miR-130a-3p mimic to overexpress miR-130a-3p. As shown in Fig. 3B, miR-130a-3p mimic resulted in a 5-fold increase in miR-130a-3p expression (p<0.0001) (Fig. 3B). Further dual-luciferase reporter assay showed that miR-130a-3p overexpression decreased the luciferase activity of the luciferase plasmid carrying WT-circSDHC but not the luciferase plasmid carrying MUT-circSDHC (p<0.0001) (Fig. 3C). To verify the effect of circSDHC on miR-130a-3p expression, oe-circSDHC was transfected into RCC cells to overexpress circSDHC, and transfection efficiency of oe-circSDHC is exhibited in Fig. 3D (p<0.0001). We observed that ectopic expression of circSDHC repressed miR-130a-3p expression, whereas circSDHC knockdown had the opposite effect (p<0.0001) (Fig. 3E). Relative expression of miR-130a-3p in RCC samples and cell lines was detected. As expected, miR-130a-3p was markedly downregulated in RCC samples and cells (p<0.0001) (Fig. 3F,G). Collectively, circSDHC served as a miR-130a-3p decoy.

CircSDHC regulated RCC cell malignant phenotypes and angiogenesis by functioning as a miR-130a-3p sponge

Considering that circSDHC served as a miR-130a-3p decoy, we further explored whether circSDHC regulated malignant phenotypes and angiogenesis of RCC cell lines through adsorbing miR-130a-3p. RCC cell lines were co-transfected with si-circSDHC and

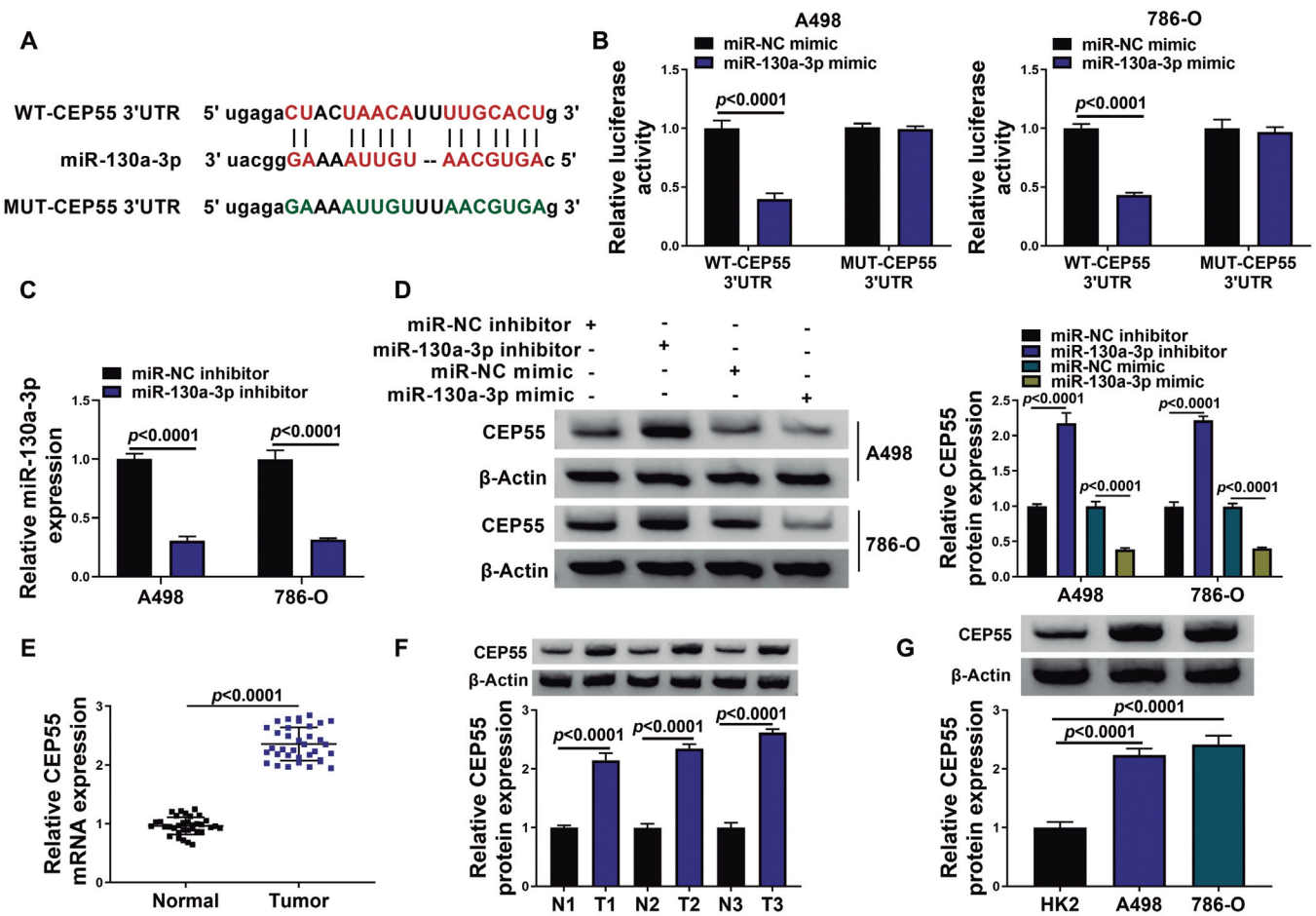

Fig. 5. CEP55 served as a miR-130a-3p target. **A.** Binding region of CEP55 with miR-130a-3p. **B.** The interaction between CEP55 and miR-130a-3p in RCC cell lines was analyzed. **C.** RT-qPCR analysis of miR-130a-3p expression in RCC cell lines with miR-130a-3p inhibitor or miR-NC inhibitor. **D.** Western blotting was utilized to measure the relative protein level of CEP55 in RCC cell lines following miR-130a-3p overexpression or silencing. **E.** Relative levels of CEP55 mRNA in RCC tissues. **F, G.** Western blotting was carried out to evaluate CEP55 protein levels in RCC tissues and cell lines. ****P<0.0001.

miR-130a-3p inhibitor. RT-qPCR displayed that the elevated expression of miR-130a-3p in RCC cells urged by circSDHC silencing was partly overturned after miR-130a-3p inhibitor transfection (p<0.0001) (Fig. 4A). Moreover, miR-130a-3p silencing reversed circSDHC knockdown-mediated impacts on RCC cell proliferation (p<0.0001 and p=0.0001) and apoptosis (p<0.0001) (Fig. 4B,C). Furthermore, inhibition of miR-130a-3p reversed the decreased protein levels of Bcl-2 (p=0.0003, p=0.0002, and p<0.0001) and the elevated protein levels of Bax (p<0.0001) in cells caused by circSDHC knockdown (Fig. 4D-F). In addition, the inhibitory effects of circSDHC silencing on angiogenesis, migration, and invasion of RCC cell lines were partly counteracted by miR-130a-3p downregulation (p<0.0001) (Fig. 4G-I). In sum, these results manifested that circSDHC mediated RCC cell malignant phenotypes and angiogenesis via miR-130a-3p.

MiR-130a-3p directly targeted CEP55

To investigate the underlying regulatory mechanism of miR-130a-3p, candidate targets were predicted using starbase database. As exhibited in Fig. 5A, CEP55 might interact with miR-130a-3p. The results showed that miR-130a-3p overexpression observably decreased the luciferase activity of the luciferase reporter containing WT-CEP55 3'UTR instead of the luciferase reporter containing MUT-CEP55 3'UTR (p<0.0001) (Fig. 5B). We then explored the effects of miR-130a-3p mimic and inhibitor on CEP55 protein levels. There was a significant downregulation of miR-130a-3p in RCC cells after transfection with miR-130a-3p inhibitor (p<0.0001) (Fig. 5C). The results suggested that miR-130a-3p overexpression repressed CEP55 protein levels, but miR-130a-3p silencing elevated CEP55 protein levels in RCC cells (p<0.0001) (Fig. 5D). The levels of CEP55 mRNA and protein in RCC samples and cells were analyzed. As expected, the mRNA and protein levels of CEP55 were higher in RCC tissues in contrast to paired normal tissues (p<0.0001) (Fig. 5E,F). Similarly, CEP55 protein levels were also increased in RCC cell lines relative to the control cell line (p<0.0001) (Fig. 5G). Together, CEP55 acted as a miR-130a-3p target.

MiR-130a-3p regulated RCC cell malignant phenotypes and angiogenesis via targeting CEP55

Whether CEP55 is involved in malignant phenotypes and angiogenesis of RCC cell lines mediated

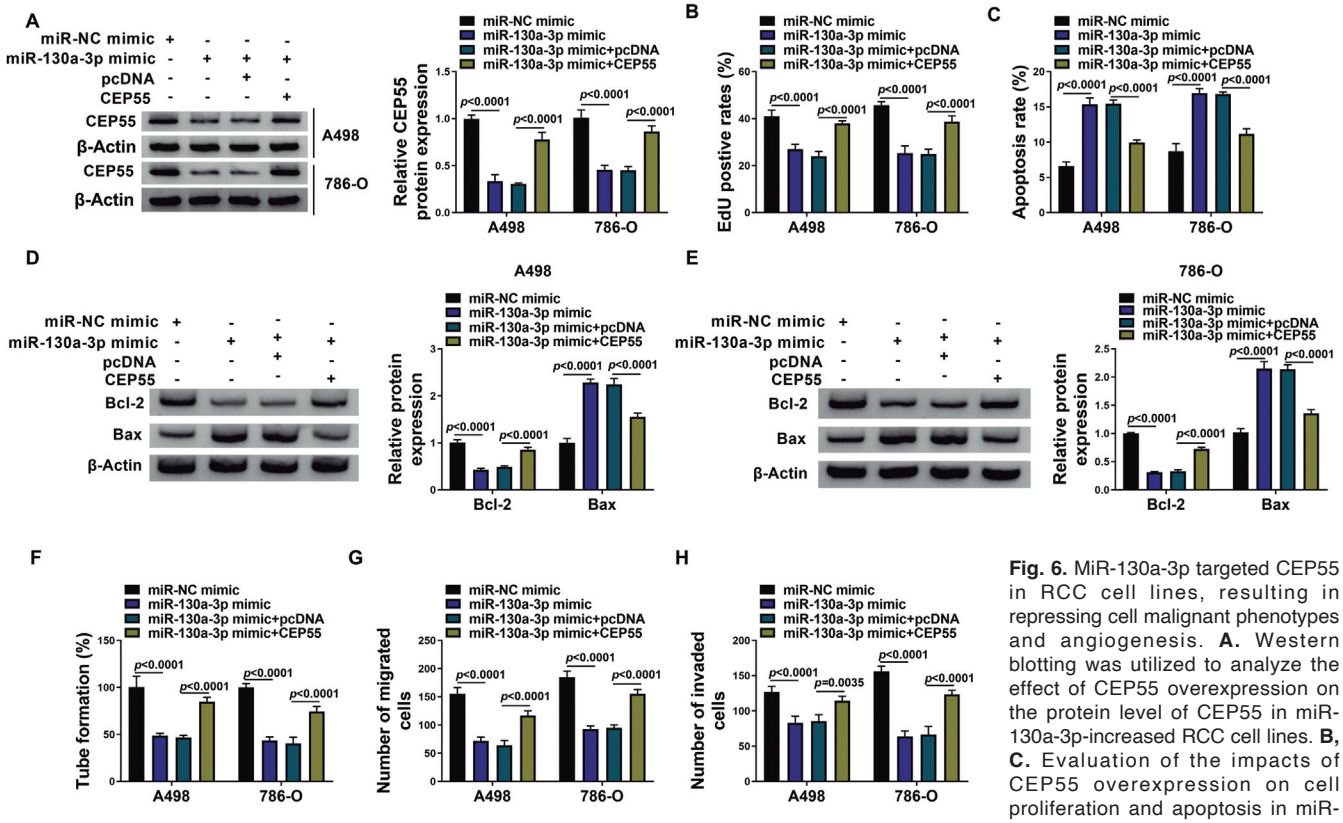

Fig. 6. MiR-130a-3p targeted CEP55 in RCC cell lines, resulting in repressing cell malignant phenotypes and angiogenesis. **A.** Western blotting was utilized to analyze the effect of CEP55 overexpression on the protein level of CEP55 in miR-130a-3p-increased RCC cell lines. **B, C.** Evaluation of the impacts of CEP55 overexpression on cell proliferation and apoptosis in miR-130a-3p-increased cells using EdU and flow cytometry assays. **D, E.** Western blotting analysis of the effects of CEP55 overexpression on Bcl-2 and Bax protein levels in miR-130a-3p-increased cells. **F-H.** Determination of the impacts of CEP55 overexpression on cell angiogenesis, migration, and invasion in miR-130a-3p-increased cells using HUVEC tube formation and transwell assays. **P<0.01 and ****P<0.0001.

by miR-130a-3p was further probed into through rescue experiments. RCC cell lines were co-transfected with miR-130a-3p mimic and the CEP55 overexpression plasmid. The repressive impact of miR-130a-3p overexpression on CEP55 protein levels was partly offset after transfection with CEP55 overexpression plasmid $p<0.0001$) (Fig. 6A). Moreover, miR-130a-3p overexpression restrained cell proliferation and induced cell apoptosis in RCC cell lines, but these impacts caused by miR-130a-3p overexpression were overturned after the introduction of the CEP55 overexpression plasmid ($p<0.0001$) (Fig. 6B,C). Also, CEP55 overexpression reversed the changes in Bax and Bcl-2 protein levels in RCC cell lines mediated by exogenous expression of miR-130a-3p ($p<0.0001$) (Fig. 6D,E). In addition, exogenic expression of CEP55 reversed miR-130a-3p mimic-mediated suppression on RCC cell angiogenesis ($p<0.0001$), migration ($p<0.0001$), and invasion ($p=0.0035$ and $p<0.0001$) (Fig. 6F-H). Together, miR-130a-3p curbed malignant phenotypes and angiogenesis of RCC cell lines by targeting CEP55.

CircSDHC regulated CEP55 expression by sponging miR-130a-3p

We further analyzed whether circSDHC regulated CEP55 expression by sponging miR-130a-3p. The results showed that circSDHC inhibition decreased CEP55 protein levels in RCC cell lines, but this decrease was partly reversed after miR-130a-3p silencing ($p<0.0001$) (Fig. 7A-C). In contrast, circSDHC overexpression increased CEP55 protein levels, but this change was overturned after miR-130a-3p upregulation ($p=0.0008$ and $p<0.0001$) (Fig. 7D-F). Pearson's correlation analysis showed a negative correlation between circSDHC and miR-130a-3p expression levels in RCC samples ($r=-0.8276$ and $p<0.0001$) (Fig. 7G). In addition, we also observed that the expression of CEP55

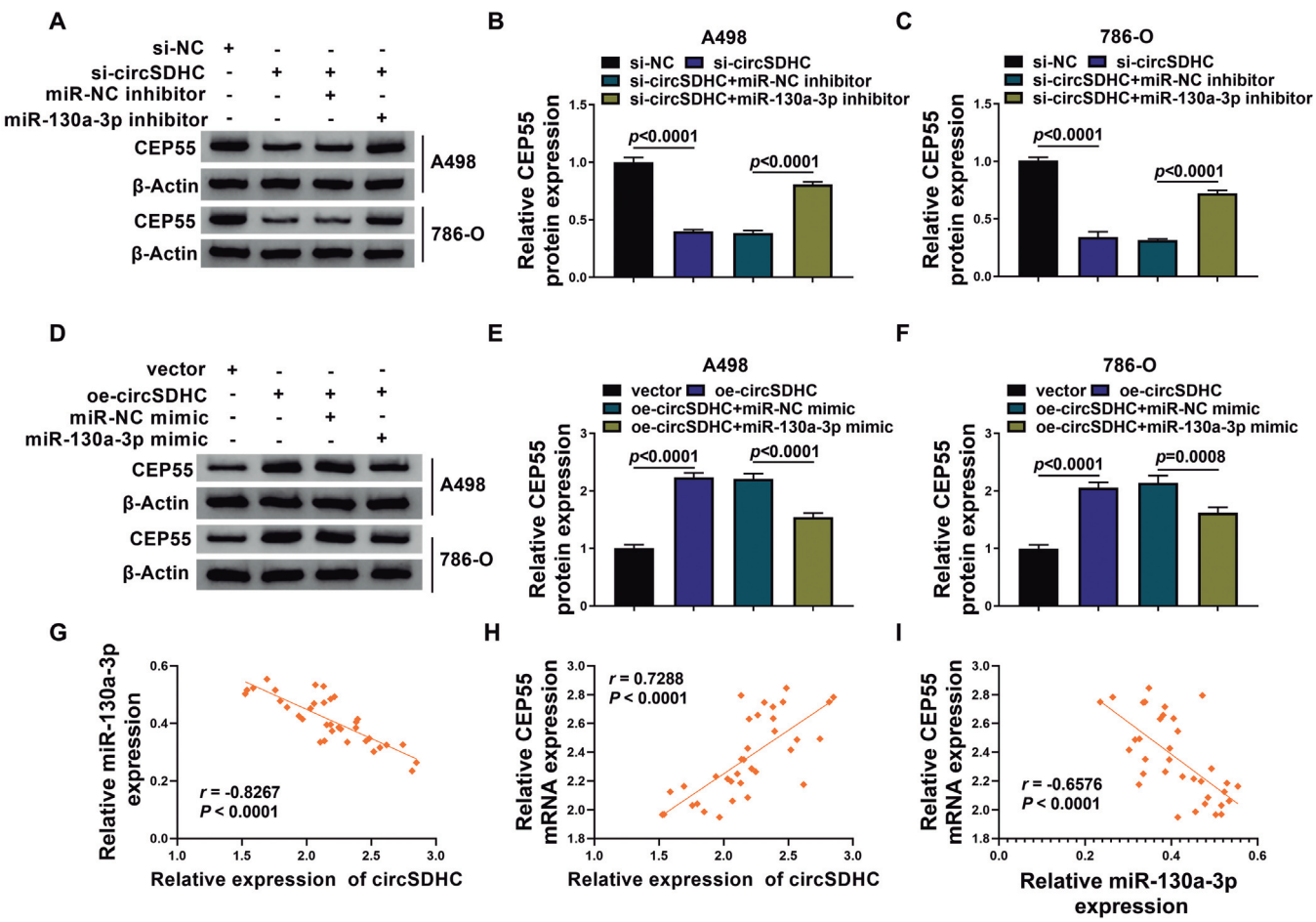

Fig. 7. CircSDHC regulated CEP55 expression by functioning as a miR-130a-3p sponge. **A-C.** Western blotting was utilized to evaluate the effect of miR-130a-3p inhibition on CEP55 protein levels in circSDHC-silenced RCC cell lines. **D-F.** Western blotting was executed to analyze the influence of miR-130a-3p mimic on CEP55 protein levels in circSDHC-overexpressed RCC cells. **G-H.** Pearson's correlation analysis assessed the correlation among circSDHC, miR-130a-3p, and CEP55 mRNA expression levels in RCC samples. ***$P<0.001$ and ****$P<0.0001$.

mRNA was positively correlated with circSDHC (r=0.7288 and p<0.0001) and negatively correlated with miR-130a-3p (r=-0.6576 and p<0.0001) in RCC samples (Fig. 7H,I). In sum, circSDHC regulated CEP55 expression through sponging miR-130a-3p.

CircSDHC silencing decreased RCC cell growth in vivo

We then demonstrated the oncogenic effect of circSDHC through *in vivo* experiments. The results showed that the volume and weight of xenograft tumors in the circSDHC-knockdown group were overtly smaller and lower than the control group (p<0.0001) (Fig. 8A,B). RT-qPCR showed that circSDHC and CEP55 levels were lower in xenograft tumors from the sh-circSDHC group, but miR-130a-3p levels were higher (p<0.0001) (Fig. 8C-E). IHC analysis presented that CEP55 levels were also decreased in xenograft tumors from the sh-circSDHC group (Fig. 8F). These results manifested that circSDHC silencing restrained tumor growth *in vivo*.

Discussion

Recently, a handful of studies have focused on the biological functions of circRNAs in RCC. Emerging evidence indicates that deregulation of some circRNAs is involved in the tumorigenesis of RCC (Wang et al., 2020). Currently, the regulatory mechanism of circRNAs in RCC is unclear. Herein, we verified that circSDHC functioned as a miR-130a-3p sponge and promoted malignant phenotypes and angiogenesis of RCC cells by increasing CEP55 expression via sequestering miR-130a-3p.

Angiogenesis, the formation of new blood vessels from original blood vessels, is a vital event in blood metastasis and tumor growth (Li et al., 2019). Also, angiogenesis is considered to be a hallmark of solid tumors (Majidpoor and Mortezaee, 2021). Angiogenesis plays a key role in the pathophysiology of RCC (Billemont et al., 2007). Angiogenesis-related mechanisms represent an important RCC biology and one of the most effective treatments for advanced renal

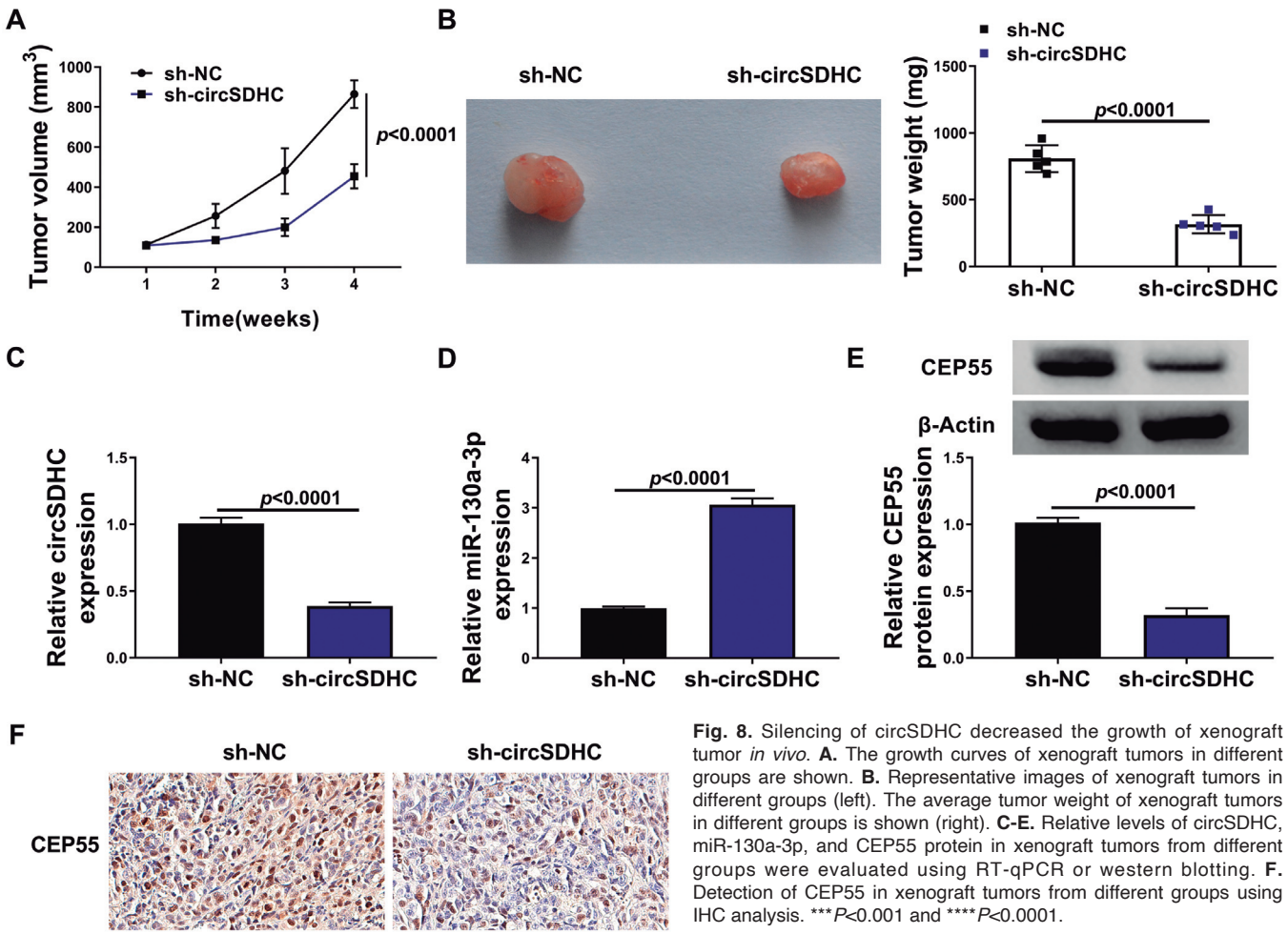

Fig. 8. Silencing of circSDHC decreased the growth of xenograft tumor *in vivo*. **A.** The growth curves of xenograft tumors in different groups are shown. **B.** Representative images of xenograft tumors in different groups (left). The average tumor weight of xenograft tumors in different groups is shown (right). **C-E.** Relative levels of circSDHC, miR-130a-3p, and CEP55 protein in xenograft tumors from different groups were evaluated using RT-qPCR or western blotting. **F.** Detection of CEP55 in xenograft tumors from different groups using IHC analysis. ***P<0.001 and ****P<0.0001.

tumors is angiogenesis inhibition (Argentiero and Solimando, 2020). Herein, circSDHC levels were higher in RCC samples and cells. Silencing of circSDHC decreased xenograft tumor growth *in vivo* and induced RCC cell apoptosis and restrained RCC cell proliferation, angiogenesis, migration, and invasion *in vitro*. Cen et al. manifested that circSDHC overexpression was associated with poor survival and advanced TNM stage in RCC patients, and circSDHC silencing curbed RCC cell metastasis and proliferation via regulating the CDKN3/E2F1 axis by functioning as a miR-127-3p sponge (Cen et al., 2021). These results manifested that circSDHC promoted cell malignant phenotypes and angiogenesis in RCC.

Sponging miRNAs is one of the significant functions of circRNAs (Hansen et al., 2013). Most circRNAs possess one or more miRNA recognition elements (MREs), which bind to miRNAs to regulate miRNA-targeted genes (Xu et al., 2018). Here, we used a bioinformatics database to predict that circSDHC might be a miR-130a-3p sponge. Intriguingly, miR-130a-3p overexpression decreased the luciferase intensity of the WT-circSDHC reporter. In RCC cell lines, circSDHC overexpression repressed miR-130a-3p expression, but circSDHC inhibition elevated miR-130a-3p expression. These results proved circSDHC as a miR-130a-3p sponge. A previous study manifested that CCAT1 contributed to clear cell RCC cell invasion and proliferation via negatively regulating miR-130a-3p expression (Jing et al., 2021). Also, circRNA-0054537 sequestered miR-130a-3p and elevated cMet expression, resulting in contributing to RCC cell migration and proliferation (Li et al., 2020b). Herein, miR-130a-3p inhibitor offset the suppressive effects of circSDHC silencing on RCC cell malignant phenotypes and angiogenesis, manifesting that circSDHC regulated RCC cell malignant phenotypes and angiogenesis through sponging miR-130a-3p.

CEP55 is a key effector of both midbody formation and midbody remnant degradation (Sardina et al., 2020). High CEP55 expression is correlated with clinic-pathological parameters across multiple human cancers, such as colorectal cancer (Huang et al., 2021), esophageal squamous cell cancer (Yan et al., 2021), and breast cancer (He et al., 2021). In RCC-related studies, Feng et al. manifested that circRNA-001287 promoted RCC progression by regulating CEP55 expression (Feng et al., 2020). Chen et al. reported that CEP55 promoted RCC cell epithelial-mesenchymal transition (Chen et al., 2019). Our results proved CEP55 as a miR-130a-3p target. Moreover, CEP55 upregulation counteracted miR-130a-3p-mediated repression on RCC cell malignant phenotypes and angiogenesis. Importantly, circSDHC was able to regulate CEP55 expression through adsorbing miR-130a-3p. Thus, we concluded that circSDHC regulated RCC cell malignant phenotypes and angiogenesis through modulating the miR-130a-3p/CEP55 axis.

In summary, our study provided evidence to support the involvement of circSDHC in RCC. Mechanistically, circSDHC functioned as a miR-130a-3p sponge and increased CEP55 expression through adsorbing miR-130a-3p, thus promoting RCC cell malignant phenotypes and angiogenesis. The study supported that circSDHC might be a promising target for RCC treatment.

Acknowledgements. None.

Disclosure of interest. The authors declare that they have no conflicts of interest.

Funding. There is no funding.

Ethical approval . The use of human clinical samples was approved by the Ethics Committee of The Fourth Hospital of Hebei Medical University and in accordance the tenets of the Helsinki Declaration.

References

Argentiero A. and Solimando A.G. (2020). Anti-angiogenesis and immunotherapy: Novel paradigms to envision tailored approaches in renal cell-carcinoma. J. Clin. Med. 9, 1594.

Billemont B., Méric J.B., Izzedine H., Taillade L., Sultan-Amar V. and Rixe O. (2007). Angiogenesis and renal cell carcinoma. Bull Cancer 94 Spec. No, S232-240 (in French).

Cen J., Liang Y., Huang Y., Pan Y., Shu G., Zheng Z., Liao X., Zhou M., Chen D., Fang Y., Chen W., Luo J. and Zhang J. (2021). Circular RNA circSDHC serves as a sponge for miR-127-3p to promote the proliferation and metastasis of renal cell carcinoma via the CDKN3/E2F1 axis. Mol. Cancer 20, 19.

Chen H., Zhu D., Zheng Z., Cai Y., Chen Z. and Xie W. (2019). CEP55 promotes epithelial-mesenchymal transition in renal cell carcinoma through PI3K/AKT/mTOR pathway. Clin. Transl. Oncol. 21, 939-949.

Ebbesen K.K., Hansen T.B. and Kjems J. (2017). Insights into circular RNA biology. RNA Biol. 14, 1035-1045.

Feng J., Guo Y., Li Y., Zeng J., Wang Y., Yang Y., Xie G. and Feng Q. (2020). Tumor promoting effects of circRNA_001287 on renal cell carcinoma through miR-144-targeted CEP55. J. Exp. Clin. Cancer Res. 39, 269.

Ghafouri-Fard S., Shirvani-Farsani Z., Branicki W. and Taheri M. (2020). MicroRNA signature in renal cell carcinoma. Front Oncol. 10, 596359.

Gudowska-Sawczuk M., Kudelski J. and Mroczko B. (2020). The role of chemokine receptor CXCR3 and its ligands in renal cell carcinoma. Int. J. Mol. Sci. 21, 8582.

Hansen T.B., Jensen T.I., Clausen B.H., Bramsen J.B., Finsen B., Damgaard C.K. and Kjems J. (2013). Natural RNA circles function as efficient microRNA sponges. Nature 495, 384-388.

He Y., Cao Y., Wang X., Jisiguleng W., Tao M., Liu J., Wang F., Chao L., Wang W., Li P., Fu H., Xing W., Zhu Z. and Huan Y. (2021). Identification of hub genes to regulate breast cancer spinal metastases by bioinformatics analyses. J. Oncol. 2021, 5548918.

Huang R.H., Yang W.K., Wu C.M., Yeh C.M. and Sung W.W. (2021). Over-expression of CEP55 predicts favorable prognosis in colorectal cancer patients with lymph node involvement. Comput. Math Methods Med. 41, 543-547.

Izumi K., Saito K., Nakayama T., Fukuda S., Fukushima H., Uehara S., Koga F., Yonese J., Kageyama Y. and Fujii Y. (2020). Contact with renal sinus is associated with poor prognosis in surgically treated pT1 clear cell renal cell carcinoma. Int. J. Urol. 27, 657-662.

Jeffery J., Sinha D., Srihari S., Kalimutho M. and Khanna K.K. (2016). Beyond cytokinesis: the emerging roles of CEP55 in tumorigenesis. Oncogene 35, 683-690.

Jin J., Sun H., Shi C., Yang H., Wu Y., Li W., Dong Y.H., Cai L. and Meng X.M. (2020). Circular RNA in renal diseases. J. Cell Mol. Med. 24, 6523-6533.

Jing J., Zhao X., Wang J. and Li T. (2021). Potential diagnostic and prognostic value and regulatory relationship of long noncoding RNA CCAT1 and miR-130a-3p in clear cell renal cell carcinoma. Cancer Cell Int. 21, 68.

Kovacova J., Poprach A., Buchler T., Cho W.C. and Slaby O. (2018). MicroRNAs as predictive biomarkers of response to tyrosine kinase inhibitor therapy in metastatic renal cell carcinoma. Clin. Chem. Lab. Med. 56, 1426-1431.

Kristensen L.S., Andersen M.S., Stagsted L.V.W., Ebbesen K.K. and Hansen T.B. (2019). The biogenesis, biology and characterization of circular RNAs. Nat. Rev. Genet. 20, 675-691.

Lee H.H., Elia N., Ghirlando R., Lippincott-Schwartz J. and Hurley J.H. (2008). Midbody targeting of the ESCRT machinery by a noncanonical coiled coil in CEP55. Science 322, 576-580.

Lee J.C., Yotis D.M., Lee J.Y., Sarabusky M.A., Shrum B., Champagne A., Ismail O.Z., Tutunea-Fatan E., Leong H.S. and Gunaratnam L. (2021). Kidney injury molecule-1 inhibits metastasis of renal cell carcinoma. Sci. Rep. 11, 11840.

Li S., Xu H.X., Wu C.T., Wang W.Q., Jin W., Gao H.L., Li H., Zhang S.R., Xu J.Z., Qi Z.H., Ni Q.X., Yu X.J. and Liu L. (2019). Angiogenesis in pancreatic cancer: current research status and clinical implications. Angiogenesis 22, 15-36.

Li J., Huang C., Zou Y., Ye J., Yu J. and Gui Y. (2020a). CircTLK1 promotes the proliferation and metastasis of renal cell carcinoma by sponging miR-136-5p. Mol. Cancer 19, 103.

Li R., Luo S. and Zhang D. (2020b). Circular RNA hsa_circ_0054537 sponges miR-130a-3p to promote the progression of renal cell carcinoma through regulating cMet pathway. Gene 754, 144811.

Liu H., Hu G., Wang Z., Liu Q., Zhang J., Chen Y., Huang Y., Xue W., Xu Y. and Zhai W. (2020). circPTCH1 promotes invasion and metastasis in renal cell carcinoma via regulating miR-485-5p/MMP14 axis. Theranostics 10, 10791-10807.

Majidpoor J. and Mortezaee K. (2021). Angiogenesis as a hallmark of solid tumors - clinical perspectives. Cell Oncol. (Dordr) 44, 715-737.

Miricescu D., Balan D.G., Tulin A., Stiru O., Vacaroiu I.A., Mihai D.A., Popa C.C., Papacocea R.I., Enyedi M., Sorin N.A., Vatachki G., Georgescu D.E., Nica A.E. and Stefani C. (2021). PI3K/AKT/mTOR signalling pathway involvement in renal cell carcinoma pathogenesis (Review). Exp. Ther. Med. 21, 540.

Nogueira I., Dias F., Teixeira A.L. and Medeiros R. (2018). miRNAs as potential regulators of mTOR pathway in renal cell carcinoma. Pharmacogenomics 19, 249-261.

Pal S.K., Ghate S.R., Li N., Swallow E., Peeples M., Zichlin M.L., Perez J.R., Agarwal N. and Vogelzang N.J. (2017). Real-world survival outcomes and prognostic factors among patients receiving first targeted therapy for advanced renal cell carcinoma: A SEER-medicare database analysis. Clin. Genitourin. Cancer 15, e573-e582.

Petejova N. and Martinek A. (2016). Renal cell carcinoma: Review of etiology, pathophysiology and risk factors. Biomed. Pap. Med. Fac. Univ. Palacky Olomouc. Czech Repub. 160, 183-194.

Roberto M., Botticelli A., Panebianco M., Aschelter A.M., Gelibter A., Ciccarese C., Minelli M., Nuti M., Santini D., Laghi A., Tomao S. and Marchetti P. (2021). Metastatic renal cell carcinoma management: From molecular mechanism to clinical practice. Front. Oncol. 11, 657639

Santer L., Bär C. and Thum T. (2019). Circular RNAs: A novel class of functional RNA molecules with a therapeutic perspective. Mol. Ther. 27, 1350-1363.

Sardina F., Monteonofrio L., Ferrara M., Magi F., Soddu S. and Rinaldo C. (2020). HIPK2 is required for midbody remnant removal through autophagy-mediated degradation. Front. Cell Dev. Biol. 8, 572094.

Suzuki H., Zuo Y., Wang J., Zhang M.Q., Malhotra A. and Mayeda A. (2006). Characterization of RNase R-digested cellular RNA source that consists of lariat and circular RNAs from pre-mRNA splicing. Nucleic Acids Res. 34, e63.

Tandon D. and Banerjee M. (2020). Centrosomal protein 55: A new paradigm in tumorigenesis. Eur. J. Cell Biol. 99, 151086.

Wang H., Huo X., Yang X.R., He J., Cheng L., Wang N., Deng X., Jin H., Wang N., Wang C., Zhao F., Fang J., Yao M., Fan J. and Qin W. (2017). STAT3-mediated upregulation of lncRNA HOXD-AS1 as a ceRNA facilitates liver cancer metastasis by regulating SOX4. Mol. Cancer 16, 136.

Wang Y., Zhang Y., Wang P., Fu X. and Lin W. (2020). Circular RNAs in renal cell carcinoma: implications for tumorigenesis, diagnosis, and therapy. Mol. Cancer 19, 149.

Xu S., Zhou L. and Ponnusamy M. (2018). A comprehensive review of circRNA: from purification and identification to disease marker potential. Peer J. 6, e5503.

Yan S.M., Liu L., Gu W.Y., Huang L.Y., Yang Y. and Huang Y.H. (2021). CEP55 positively affects tumorigenesis of esophageal squamous cell carcinoma and is correlated with poor prognosis. J. Oncol. 2021, 8890715.

Zhong G., Lin Y., Wang X., Wang K. and Liu J. (2020). H19 knockdown suppresses proliferation and induces apoptosis by regulating miR-130a-3p/SATB1 in breast cancer cells. Onco. Targets Ther. 13, 12501-12513.

Zhou L., Liu S., Li X., Yin M., Li S. and Long H. (2019). Diagnostic and prognostic value of CEP55 in clear cell renal cell carcinoma as determined by bioinformatics analysis. Mol. Med. Rep. 19, 3485-3496.

Zhu J., Luo Y., Zhao Y., Kong Y., Zheng H., Li Y., Gao B., Ai L., Huang H., Huang J., Li Z. and Chen C. (2021). circEHBP1 promotes lymphangiogenesis and lymphatic metastasis of bladder cancer via miR-130a-3p/TGFβR1/VEGF-D signaling. Mol. Ther. 29, 1838-1852.

Accepted May 4, 2022